How to cite: *Angew. Chem. Int. Ed.* **2021**, *60*, 10147–10154
International Edition: doi.org/10.1002/anie.202016608
German Edition: doi.org/10.1002/ange.202016608

Battery Materials

Stepped Channels Integrated Lithium–Sulfur Separator via Photoinduced Multidimensional Fabrication of Metal–Organic Frameworks

Guang-Kuo Gao[+], Yi-Rong Wang[+], Si-Bo Wang[+], Ru-Xin Yang, Yifa Chen, Yu Zhang, Cheng Jiang, Mei-Jie Wei, Huiyuan Ma, and Ya-Qian Lan**

Abstract: *Multidimensional fabrication of metal–organic frameworks (MOFs) into multilevel channel integrated devices are in high demanded for Li-S separators. Such separators have advantages in pore-engineering that might fulfill requirements such as intercepting the diffusing polysulfides and improving the Li^+/electrolyte transfer in Li-S batteries. However, most reported works focus on the roles of MOFs as ionic sieves for polysulfides while offering limited investigation on the tuning of Li^+ transfer across the separators. A photoinduced heat-assisted processing strategy is proposed to fabricate MOFs into multidimensional devices (e.g., hollow/Janus fibers, double-or triple-layer membranes). For the first time, a triple-layer separator with stepped-channels has been designed and demonstrated as a powerful separator with outstanding specific capacity (1365.0 mAh g^{-1}) and cycling performance (0.03 % fading per cycle from 100th to 700th cycle), which is superior to single/double-layer and commercial separators. The findings may expedite the development of MOF-based membranes and extend the scope of MOFs in energy-storage technologies.*

Introduction

With increasing concerns about the anthropogenic impacts of current trends in energy utilization, as well as the prospect of new energy supply to meet future needs, we are at a stage where revolutionary change of our energy paradigm is a must.[1] Battery technology is a key issue in sustainable energy conversion/storage and acting as a vital factor in limiting the development of advanced techniques like electrical vehicles, unmanned drone or smart mobile devices when taking the limited theoretical capacity of conventional lithium-ion batteries into consideration. To go beyond lithium-ion batteries and attain a higher energy density and lower cost, Li-S batteries with the advantages like high theoretical specific capacity (1675 mAh g^{-1}), high theoretical energy density (2600 Wh kg^{-1}) as well as abundant reserves and low cost of sulfur have been considered as the most promising candidates for new generation of battery system.[2,3] During past decades, much effort has been devoted to the development of Li-S battery yet the performance obtained to date has still been far from satisfactory and is still restricted by the problems like the formation of polysulfides (Li_2S_n; n = 2–8) with complex electrochemical reaction kinetics and shuttling effect;[4,5] cell-polarization caused by Li^+/electrolyte transfer[6,7] and the formation of lithium dendrite,[8,9] etc. Most of these problems are closely related to the bottlenecks of separator (an important component of the battery that is responsible for separating the cathode and anode to avoid short-circuiting while allowing transport of conducting ions in the electrolyte) and might be conquered with the development of advanced separator technology. Specially, a powerful Li-S separator needs to satisfy the properties like: 1) high barrier properties to block the shuttling effect of polysulfides;[10] 2) certain pore size or good wettability to achieve high passage efficiency for both Li^+ ions and electrolyte[11] and 3) high stability or self-healing properties that can resist electrolyte corrosion, endure the formation of lithium dendrites and provide automatic shutdown protection.[12,13] To this end, the exploration of powerful separators that can fulfill most of these requirements of Li-S battery is long-sought-after.

In recent years, the prosperous development of Li-S batteries has witnessed the higher requirements for the separators and various porous materials (e.g., zeolites,[14] porous carbon,[15] metal oxides,[16] porous coordination polymers,[17] etc.) have been investigated. Among them, metal–organic frameworks (MOFs)-based mixed matrix membranes

[*] Dr. G.-K. Gao,[+] Prof. Y. Chen, Prof. Y.-Q. Lan
School of Chemistry, South China Normal University
Guangzhou 510006 (P. R. China)
E-mail: chyf927821@163.com
yqlan@m.scnu.edu.cn
Homepage: http://www.yqlangroup.com/
Dr. G.-K. Gao,[+] Dr. Y.-R. Wang,[+] S.-B. Wang,[+] Dr. R.-X. Yang, Prof. Y. Chen, Dr. Y. Zhang, Dr. C. Jiang, Dr. M.-J. Wei, Prof. Y.-Q. Lan
Jiangsu Key Laboratory of Biofunctional Materials, School of Chemistry and Materials Science, Nanjing Normal University
Nanjing 210023 (P. R. China)
E-mail: yqlan@njnu.edu.cn
Dr. G.-K. Gao,[+] Prof. H. Ma
School of Materials Science and Engineering, College of Chemical and Environmental Engineering
Harbin University of Science and Technology
Harbin 150040 (P. R. China)
Prof. Y. Chen
Changzhou Institute of Innovation & Development
Nanjing Normal University
Nanjing 210023 (P. R. China)
[+] These authors contributed equally to this work.
Supporting information and the ORCID identification number(s) for the author(s) of this article can be found under: https://doi.org/10.1002/anie.202016608.

(MMMs), combining the advantages of MOFs and polymers, have showed much promise in the applications of Li-S separators.[18,19] In detail, the following properties of MOFs might be vital in this field: 1) the developed pore structure of MOFs can accommodate a variety of liquid molecules like electrolyte solution, serving as ionic sieves in battery to realize low internal resistance and high ionic conductivity;[20] 2) the pore sizes of MOFs can be specially designed to block the passage of polysulfides through the size barrier, thereby increasing the diffusion resistance of polysulfides[21] and 3) many MOFs structures contain open metal sites or functional groups that might effectively mitigate the shuttling effect of polysulfides.[20] Similarly, polymers (e.g., polydimethyl siloxane (PDMS), polyethylene glycol (PEG), or cellulose, etc.) with polar functional groups like Si-O, C-O-C or -OH have also proven to be beneficial for Li^+ transmission or inhibition of polysulfides shuttling, etc.[11,22] Therefore, the most promising MOF-based MMMs for Li-S separators would be the one that can integrate MOFs with functional polymers in robust architectures, which can simultaneously conquer the crystalline/fragile nature of MOFs crystals and meet the desired requirements of Li-S separators. Up to date, the applications of MOF-based MMMs in Li-S separators are still in its fancy and methods like electrospinning, casting or vacuum filtration have been applied.[23–26] Nevertheless, most of the fabrication forms are simple and works reported to date generally apply one kind of MOF or polymer, which are hard to fulfill most of the requirements for Li-S separators. Besides, most of works focus on the roles of MOFs as ionic sieves towards polysulfides migrating to the anode while having limited investigation on the tuning of Li^+ transfer efficiency across the MOF-based separators. Some articles have reported that the fabrication of sophisticated devices like double-layer coatings on the lithium metal electrode can effectively inhibit the lithium dendrites formation with largely improved Li^+ transfer efficiency.[27,28] This illuminates a novel point for us to design MOF-based MMMs with multifunctionality and sophisticated architectures that might possess unique and superior properties over conventional MOF-based Li-S separators.

To this end, we intend to design a kind of MOF-based MMMs with stepped channels and serve it as a novel toolbox for the investigation of Li-S separator (Figure 1). In the applications of Li-S separators, there is a balance between the polysulfides inhibition, Li^+ transfer and cell polarization. For single-layer MOF-based MMMs, small pore sizes are beneficial for suppressing polysulfides yet are generally lack in Li^+/electrolyte transfer. On the contrary, single-layer MOF-based MMMs with large pore sizes might possess opposite effect on polysulfides inhibition and Li^+/electrolyte transfer (Figure 1). To conquer the limited functionality of single-layer MMMs, double-layer MMMs would be more desired to simultaneously inhibit polysulfides shuttling and facilitate the efficient transfer of Li^+/electrolyte. However, double-layer MOF-based MMMs with two kinds of pore channels integrated in a system might still face the problem like cell polarization owing to the unbalanced transfer efficiency of Li^+/electrolyte during the discharge–charge process. In this regard, MOF-based triple-layer MMMs with symmetrical stepped channels would be an alternative strategy, in which the specially designed device might efficiently suppress the cell polarization through reversible and fast transfer of Li^+/electrolyte coupling with the remained polysulfides inhibition functions (Figure 1). Therefore, methods that can integrate various MOFs in a system for Li-S separators with such structures and conquer the brittle nature of MOFs to fabricate into required shapes are particularly urgent and necessary before they can be widely adopted in practical application situations. Up-to-now, available complex MOF-based devices are limited to less than a handful of material families such as MOF-on-MOF 2D heterojunction, double-layer membranes or hollow tubes through methods like layer-by-layer,[29] casting[30] or freeze-drying,[31] etc. The fabrication of diverse MOFs integrated MMMs with stepped channels that possess synergistic effect on Li-S performance are much desired yet still largely unmet.

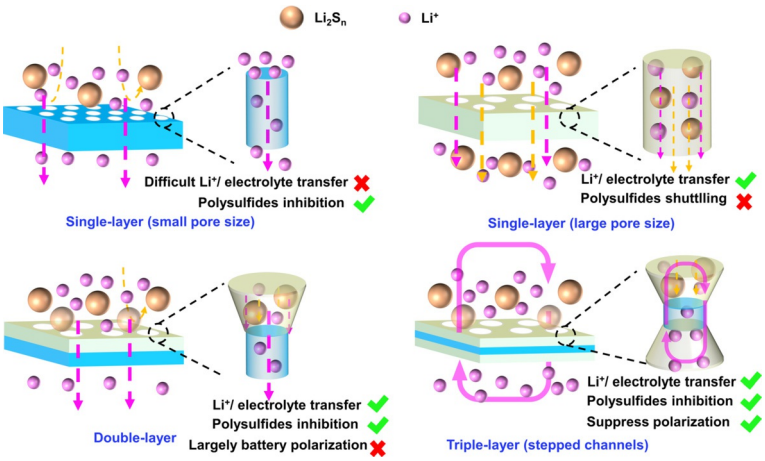

Figure 1. Representation of various MOF-based separators in the application of a Li-S cell.

Herein, we propose a two-step photoinduced heat-assisted processing (PHAP) method that can combine photoinduced shaping and heat-assisted solidification in a protocol, in which the two-step processing method enables shaping of MOFs into diverse devices (e.g., fiber, hollow tube, Janus hollow tube and double-layer/triple-layer membrane, etc.). Combining the advantages of photopolymerization polymer and MOFs together, they possess excellent robustness, flexibility, compatibility and self-healing properties. Specifically, for the first time, a kind of MOF-based triple-layer separator with stepped channels has been readily fabricated through the photoinduced multidimensional fabrication of MOFs and it exhibits boosted specific capacity (1365.0 mAh g^{-1}) and cycling performance (0.03% fading per cycle from 100th to 700th cycle), superior to single-layer/double-layer separators and commercial polypropylene (PP). This work demonstrates the concept of rational construction of triple-layer structured separators for boosted Li-S performance and provide a novel point for the applications of MOF-based devices in energy storage. Considering the diversity of

MOFs species with various pore sizes and channels, the discovery of integrated combinations of MOFs hosts for multifunctional targets is expected.

Results and Discussion

The two-step photoinduced heat-assisted processing (PHAP) method for the fabrication of MOF-based devices is illustrated in Figure 2 A and it can be concluded into three steps: dispersion of MOF nanoparticles (NPs) in monomer solution (a mixed solution of silicone and 2-hydroxyethyl acrylate (HEA)), photoinduced shaping and heat-assisted solidification. Firstly, various kinds of MOF NPs, including Zr-, Cu-, Zn- and Ce-based MOFs, have been synthesized and activated. After that, pre-activated MOF NPs with open pore channels are uniformly dispersed in monomer solution through ultrasonic. In order to achieve desired shapes, different molds like quartz hollow tune or Teflon mold have been filled with the dispersion solution. After immediate treating with a xenon lamp (wavelengths, 300 to 400 nm) to irradiate the photopolymerization process, the shaped hydrogel with molded shape is peeled off and transferred to an oven. After heating at 60 °C for 12 h, MOF-based devices with various shapes (e.g., fiber, hollow tube, membrane) and even complex devices (e.g., Janus hollow tube, two-part hollow tube, double-layer or triple-layer membrane) have been obtained.

Based on this method, various kinds of MOFs can be readily processed into different MOF-based devices. As one of the most applicable forms, MOF-based MMMs have been firstly selected as the desired model to study the feasibility of this method. Taking UiO-66@Silicone/PHEA (denoted as UiO-66@SP) as an example, the powder X-ray diffraction (PXRD) of the UiO-66@SP membrane is consistent with the original UiO-66, indicating that it can retain the inherent crystallinity and topology after the two-step PHAP process (Supporting Information, Figure S1A). Moreover, Fourier transform infrared spectroscopy (FT-IR) tests have been conducted to study the components of the materials (Figure S1B). The peaks at 1730 cm^{-1} and 1035 cm^{-1} are ascribed to the stretching variation of C=O and C-O-C bonds for ester groups of PHEA. Peaks at 1080 cm^{-1} and 1120 cm^{-1} are considered as the stretching variation of Si-O-Si bond in siloxane and peaks at 1500 cm^{-1} and 1580 cm^{-1} are the benzene ring stretching vibrations of the ligand in UiO-66. The FT-IR and PXRD results indicate the co-existence of both UiO-66 and SP, in which the tremendous amount of polar functional groups might impart the membrane with powerful functions like self-healing, ion conducting or inhibition of polysulfides shuttling. The scanning electron microscopy (SEM) image shows the good dispersal of UiO-66 NPs (diameter, ≈50 nm) on the surface of UiO-66@SP (Figure S1C). Besides, the loadings of UiO-66 can be well-tuned from ≈8 to ≈24 wt% with intact topology and high uniformity as supported by the PXRD and SEM tests (Figures S2 and S3).

To prove the versatility of this method, we further extend this method to various representative MOFs. Except for UiO-66, different MOF systems including Zr-based MOFs (e.g., NH_2-UiO-66, MOF-808 and MOF-801), Cu-based MOFs (e.g., HKUST-1), Zn-based MOFs (e.g., ZIF-8) and Ce-based MOFs (e.g., Ce-BTB) have also been explored and characterized by PXRD, SEM and FT-IR tests (Figures S4 and S5). These membranes produced from the two-step PHAP method that interweaving MOFs with functional SP, would possess high robustness owing to the strong interaction between them. To verify it, tensile stress tests are performed to show

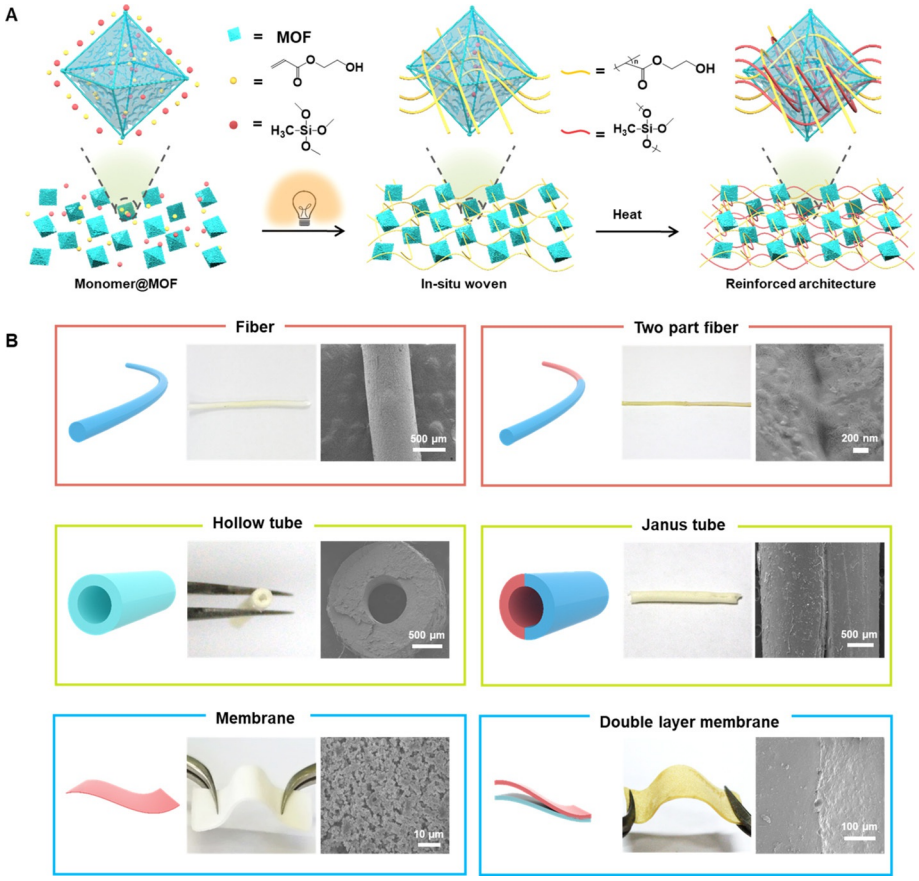

Figure 2. The characterization of different MOF-based devices fabricated through the two-step PHAP method. A) Diagrammatic depiction of the two-step PHAP method. B) Photographic and SEM images of MOF-based devices obtained from the two-step PHAP method: fiber, UiO-66@SP; two part fiber, UiO-66/NH_2-UiO-66@SP; hollow tube, UiO-66@SP; Janus tube, ZIF-8/UiO-66@SP; membrane, UiO-66@SP and double-layer membrane, UiO-66/NH_2-UiO-66@SP.

the mechanical strength of these membranes. For instance, UiO-66@SP membranes with different UiO-66 loadings present higher mechanical strength (i.e., 8 wt%, 1.6 MPa; 16 wt%, 1.2 MPa and 24 wt%, 0.7 MPa) than pristine SP (0.5 MPa), indicating the addition of MOFs particles can increase the robustness (Figure S6). Besides, the possible relation between the structural parameters (composition, morphology and size) of MOFs NPs (e.g., UiO-66) and mechanical properties of the composite membrane have also been investigated (Figures S7–S10). Furthermore, different kinds of MOF@SP membranes display good mechanical strength, suggesting the strong interaction between MOFs and SP (Figure S11).

Self-healing ability, referring to the property that enables materials to automatically repair damage and restore to a normal state, has received extensive attention in various fields like biomedicine, soft robotics engineering or energy storage.[32,33] Processing through the two-step PHAP method, the obtained materials can combine the advantages of both functional polymers and MOFs together, which might exhibit self-healing property. To verify it, a strip of UiO-66@SP hydrogel and NH_2-UiO-66@SP hydrogel are cut in halves and then positioned to be connected together with each other. After placing in air at room temperature for 10 min, the separated two parts are reconnected as a whole (Figure S12). After heat treatment at 60 °C for 12 h, the reconnected hydrogel strip is transformed into robust membrane and exhibits high mechanical strength (stress, 0.8 MPa, strain, 144%) during the tensile stress tests, indicating the strong self-healing property for the reconnected membrane (Figure S13). The inert self-healing properties might be possibly attributed to the constructed hydrogel bonding networks between MOFs and SP with diverse functional groups (e.g., -OH or Si-O-Si groups). Moreover, N_2 sorption tests have been conducted to evaluate the porosity of the samples. For most of MOF-based MMMs, the maintenance of porosity remains a giant challenge yet still lack alternative methods. Fabricated through this method, in which the loaded monomers in the pores of MOF NPs can be partially polymerized and interwoven, large amount of defects might be created to present remained MOF porosity. Taking ZIF-8@SP as an example, ZIF-8@SP with various loadings display type II curves in the N_2 sorption tests and exhibit S_{BET} values of 48, 104 and 192 $m^2 g^{-1}$ for ZIF-8@SP with 8 wt%, 16 wt% and 24 wt% loadings through Brunner-Emmet-Teller (BET) measurements, respectively (Figure S14). Referring to the reported S_{BET} values of ZIF-8 (S_{BET}, ca. 800–1600 $m^2 g^{-1}$),[34–36] the obtained values are lower than the theoretical ones, which might be possibly attributed to the partially occupied pores of MOF NPs by SP during the two-step PHAP process (Figure S14).

Based on the superior advantages like self-healing property of the materials, more elaborate devices could be further explored with this versatile two-step PHAP method. Aside from the single-layer membrane, double-layer membrane like UiO-66/NH_2-UiO-66@SP can be fabricated through the two-step PHAP method based on the template of first-layer membrane (Figure 2B). SEM image shows the cross-section of UiO-66/NH_2-UiO-66@SP is tightly connected without any gaps or cracks (Figure 2B). Furthermore, a kind of triple-layer membrane based on ZIF-8@SP, HKUST-1@SP and NH_2-UiO-66@SP has been facilely produced through the similar strategy (Figure S15). Except for membrane, fiber, another processing form, can be easily achieved by applying a tube mold and treated under similar processing steps (Figure 2B). The obtained UiO-66@SP fiber is flexible with uniformly distributed UiO-66 NPs on the surface as proved by the SEM tests (Figure 2B). In addition, if a template is placed in the middle of tube mold, a kind of hollow tube (inner diameter, ≈0.5 mm; out diameter, ≈1.5 mm) can be produced. It displays high tensile stress as verified by the preliminary tensile test with a piece of hollow tube holding a weight (≈1 kg) downside (Figure S16). Besides, to enrich the diversity of the hollow tube, three kinds of forms (i.e., double-layer, two-part and Janus hollow tubes) have been successfully fabricated with the powerful method (Figures S17 and S18, for further detail see the Methods section in the Supporting Information). Different parts of them are tightly connected as a whole without any gaps or cracks as observed in the photo and SEM images (Figure 2B). The advantages of this powerful method combining with the tunability of MOFs or polymers might largely enrich the processing forms as multidimensional devices to meet the desired applications like Li-S separators.

Produced through this powerful method, the obtained membranes with self-healing, high robustness and remained MOFs porosity might be promising candidates as separators in Li-S cell. The advantages of these MOF@SP membranes are listed below: 1) the functional groups of -OH, Si-O-Si and C-O-C in the photopolymer can provide excellent mechanical properties and Li^+ compatibility;[37] 2) the open metal sites or functional groups of MOFs can help to inhibit the shuttling effect of polysulfides[19] and 3) the pore structures of multi-dimensional devices might be specially designed as stepped channels that are beneficial for Li^+/electrolyte transfer and polysulfides inhibition.

As a proof-of-concept, we set out to explore the applications of these stand-alone devices in Li-S battery. To investigate it, NH_2-UiO-66@SP-based membrane is selected as the desired example to be applied as separator in Li-S cell. In order to increase Li^+ conductivity and improve blocking effect of polysulfides, poly(sodium-p-styrenesulfonate) (PSS) modified MOF NPs has been further studied. NH_2-UiO-66 with different PSS loadings have been successfully synthesized as proved by PXRD and FT-IR tests (Figure S19). The PSS loadings of PSS@NH_2-UiO-66-n ($n = 1$ to 4, for further detail see the Supporting information) are determined to be from 5.22 to 15.64 wt% by energy dispersive spectrometer (EDS) spectra (Table S1). In addition, PSS-modified MOFs are decorated on PP with different casting thicknesses (250 to 1000 μm, casting thickness of the precursors) through the two-step PHAP method. Taking PSS@NH_2-UiO-66@SP@PP-2 (denoted as PNSP-2) with 250 μm casting thickness for example, the top-view SEM image of separator shows that the macro-pores of PP are fully covered and the cross-section image of PNSP-2 presents a measured thickness of ≈12 μm for the coated membrane (Figure S20). PXRD test of PNSP-2 displays remained crystalline phase of NH_2-UiO-66

(Figure S21A) and N_2 sorption curve of PSS@NH_2-UiO-66@SP exhibits a S_{BET} of 79.72 $m^2 g^{-1}$, indicating remained structure and porosity of NH_2-UiO-66 in the separator (Figure S22). Notably, the tensile strain of PNSP-2 is ≈26% increase when compared with PP (Figure S21B).

To evaluate the Li-S cell performance, PNSP with different thicknesses (casting thickness, 250 to 1000 μm and membrane thickness, ≈12 to ≈22 μm) and PSS loadings are applied as separators to investigate their cycling performance by galvanostatic charge–discharge tests at 0.5 C. For the casting thicknesses of 1000, 500 and 250 μm, PNSP-2-based Li-S cells present initial capacity of 975.6, 800.2 and 1279.2 mAh g^{-1} and the capacity of them fade to 241.4, 205 and 554.6 mAh g^{-1} after 700 cycles, respectively (Figure S23A). For the casting thickness of 75 μm, Li-S battery displays an lower initial capacity of 765 mAh g^{-1} and decreases to 415.7 mAh g^{-1} after 550 cycles (Figure S23A). This indicates 250 μm as the moderate thickness to be the best one. The reason might be the thicker of coating layer, the higher mass transfer resistance and larger battery polarization would be achieved (Figure S24). In addition, Li-S batteries assembled with the pure polymer-based separator shows much poorer performance when compared with MOF-loaded ones, which further prove the viral roles of MOFs (Figure S23C). Besides, PNSP-*n* ($n = 1$–4) with different PSS loadings are applied to investigate their cell performance. The initial capacity of PNSP-1, PNSP-3 and PNSP-4 are 1175.9, 1085.3, 1246.6 mAh g^{-1} and decreased to 484.4, 407.6, 405.2 mAh g^{-1} after 700 cycles, respectively, which are lower than PNSP-2 (Figure S23B). Besides, the results show that the addition of PSS can reduce the cell polarization (i.e., ΔE, PNSP-1, 0.33 V; PNSP-2, 0.24 V; PNSP-3, 0.22 V and PNSP-4, 0.20 V), implying PNSP-2 to be best one with high capacity and low cell polarization (Figure S25). Therefore, the best PSS loading and casting thickness have been well-defined for single-layer membrane based on the above mentioned results and the following samples are based on the similar fabrication conditions.

Due to the strong interaction between MOFs and SP, the PNSP-2-based separator might have self-healing properties that can endure damage arising from different factors like lithium dendrites penetration. To simulate and even enlarge the possible damage during the cycling process of Li-S cell, a violent penetration experiment has been conducted, during which the PNSP-2-based separator is almost cut in half (Figure S26). After UV treating for 15 min, a reconnected separator is obtained (Figure S26). The separator can be further assembled in Li-S cell to test the cycling performance. Interestingly, the initial capacity can be still remained at 925.2 mAh g^{-1} and the cell can still continue the discharge–charge cycling tests for more than 100 cycles (Figure S26). In contrast, the pure PP separators with similar cutting treatment results in intermediately short-circuit. This result proves the high robustness and self-healing properties of the separators obtained from such a powerful two-step PHAP method, which would provide strong protection to avoid a series of safety issues like lithium dendrites penetration to ensure the long cycling life under harsh conditions.

Based on the successful fabrication and superior performance of single-layer separator, MOF-based triple-layer MMMs with stepped channels can be also obtained through the two-step PHAP method. MOF-based triple-layer MMMs with stepped channels might efficiently suppress the cell polarization through reversible and fast transfer of Li^+/electrolyte and possess polysulfides inhibition functions.[38] To produce this device, two kind of MOFs with different pore apertures (i.e., NH_2-UiO-66, ≈5 Å and Ce-BTB, ≈10 Å) are selected and fabricated through the layer-by-layer PHAP method. Ce-BTB possesses 1D hexagonal channels (the aperture window is ≈10 Å) (Figure 4A), which would be beneficial for Li^+/electrolyte transfer yet still lack in the inhibition of polysulfides shuttling (polysulfides, 0.51 to 0.68 nm).[39] In contrast, NH_2-UiO-66 presents interconnected tetrahedral and octahedral cages whose faces comprise a triangular aperture (size, ≈5 Å), which might have opposite effect on Li^+/electrolyte transfer and polysulfides inhibition. Triple-layer membrane, as a powerful processing form that PSS@Ce-BTB@SP-2 is casted onto both ends of PSS@NH_2-UiO-66@SP-2, has been successfully fabricated as a desired model. In addition, single-layer membranes like PSS@NH_2-UiO-66@SP@PP-2 (PNSP-2) or PSS@Ce-BTB@SP@PP-2 (PCSP-2) and double-layer membrane based on them have also been fabricated as contrast samples. The cross-section SEM and elemental mapping images show apparent separated layers for the triple-layer membrane, in which Ce and Zr elements are uniformly distributed in each layer (Figure 3A,B). In order to study the polysulfides permeation ability of these separators, the shuttling experiments are tested. As shown in Figure S27, the deep red polysulfides solution is placed in 1.5 mL glass vial and the bottle mouth is covered by different membranes. After that, the vial mouth is immersed in the DOL/DME solution (v/v, 1:1). Interestingly, polysulfides permeation test shows that neither PNSP-2 nor triple-layer membrane can efficiently restrain the shuttling of

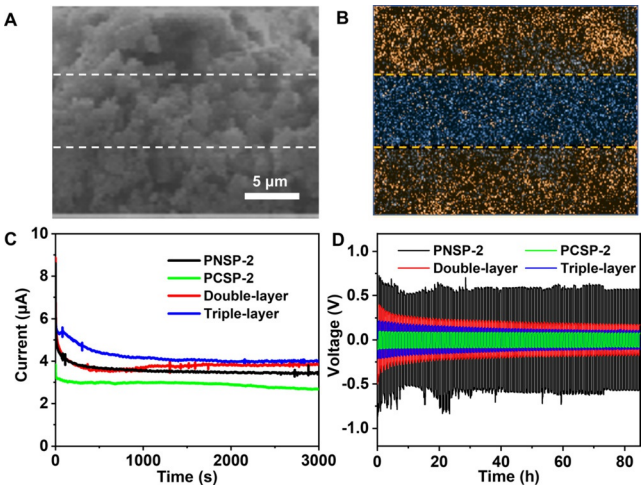

Figure 3. The characterization and symmetric cell tests of the triple-layer membrane. A) SEM image of the cross-section for the triple-layer membrane. B) EDS mapping image of the cross-section for the triple-layer membrane (Ce (orange), Zr (blue)). C) Chronoamperometry profiles for different separators. D) Galvanostatic cycling of symmetric lithium cells with different separators.

polysulfides for more than 24 h, while PCSP-2 with similar thickness can only inhibit polysulfides shuttling for less than 24 h (Figure S27). All of the results are far superior to PP, in which the permeation phenomenon occurs after only 1 h and the color of electrolyte solution changes to brown after 4 h (Figure S27).

Based on the above results, single-layer (PNSP-2 or PCSP-2), double-layer and triple-layer membranes coated onto PP are assembled as separators in coin cell with KB/S as the cathode materials and Li metal foils as anodes. To investigate the electrochemical behavior of all of these separators for Li-S cell, regular electrochemical tests, such as galvanostatic discharge–charge, cyclic voltammetry (CV) and electrochemical impedance spectra (EIS) have been conducted. CV tests are performed to study the conversion of polysulfides in the cell. Taking PNSP-2-based Li-S cell as an example, it exhibits two reduction peaks centered at 2.23 and 2.04 V, representing the reduction of elemental sulfur to soluble high order polysulfides (Li_2S_n, $4 < n < 8$) and their further reduction to solid lithium sulfides (Li_2S_2/Li_2S), respectively.[40] The broad anode peak at about 2.35 V indicates that Li_2S_2 or Li_2S is converted to sulfur during charging (Figure S28A). This phenomenon is further confirmed by galvanostatic discharge–charge curves (Figure S28C). By the way, all the samples display two cathodic peaks at 2.3 V and 2.0 V and the overlapping two anodic peaks at 2.3–2.4 V confirm the two-step redox reactions as shown in the voltage profiles (Figure S29). In addition, the weak scan peaks and increased cell polarization could be attributed to the poor Li^+ transfer efficiency and polysulfide diffusion. Besides, the EIS of the cell has been tested against all these Li-S cells with different separator systems and present similar Nyquist plots. The results show that the R_{ct} values of triple-layer-based cell has the lowest value (7.2 Ω) than that of double-layer (10.71 Ω), PNSP-2- (8.46 Ω), PCSP-2- (12.926 Ω) and pure PP-based (14.14 Ω) cells, implying a much more rapid electron transfer efficiency between electrode and electrolyte (Figure S28B; Figure 4B). Combined with the slope of the low frequency region, it can be seen that PCSP-2-based Li-S battery is more beneficial for the Li^+ diffusion in the battery. However, the semicircle in the intermediate frequency region, reflecting the charge-transfer resistance R_{ct} at the electrode interface, shows that the addition of Ce-BTB slows down the dynamic conversion process of polysulfides and cause excessive polarization. The galvanostatic discharge–charge curves of the polarization voltage shown in the second cycle also confirms this conclusion (Figure 4C).

Furthermore, the rate performance of the cell is evaluated by galvanostatic charge–discharge at various rates from 0.1 to 2 C within a potential window of 1.7–2.7 V (Figure S28D). It can be seen that the triple-layer membrane-based Li-S cell shows an initial capacity of 1296.5 mAh g^{-1} at 0.1 C, which is 350 mAh g^{-1} larger than that of PP-based Li-S cell. The additional capacity for triple-layer-based Li-S cell might be attributed to the efficient inhibition of polysulfides shuttling. With the increased current densities (i.e., 0.2, 0.5, 1 and 2 C), triple-layer-based Li-S cell delivers capacity of 1037.1, 913.9, 840.6 and 766.6 mAh g^{-1} at the rates of 0.2, 0.5, 1 and 2 C, respectively, which is also superior to PP (i.e., 667.5, 550.7, 391.1 and 301.8 mAh g^{-1} at the rates of 0.2, 0.5, 1 and 2 C, respectively; Figure S28D). Finally, the capacity of triple-layer-based Li-S cell can return to 1083.5 mAh g^{-1} at 0.1 C, showing high rate performance. In contrast, the PNSP-2-based Li-S cell displays capacity of 1146, 949.8, 853.8, 773.6 and 700.7 mAh g^{-1} from 0.1 C to 2 C and the capacity returns to 996.9 mAh g^{-1} at 0.1 C, which is lower than triple-layer-based Li-S cell.

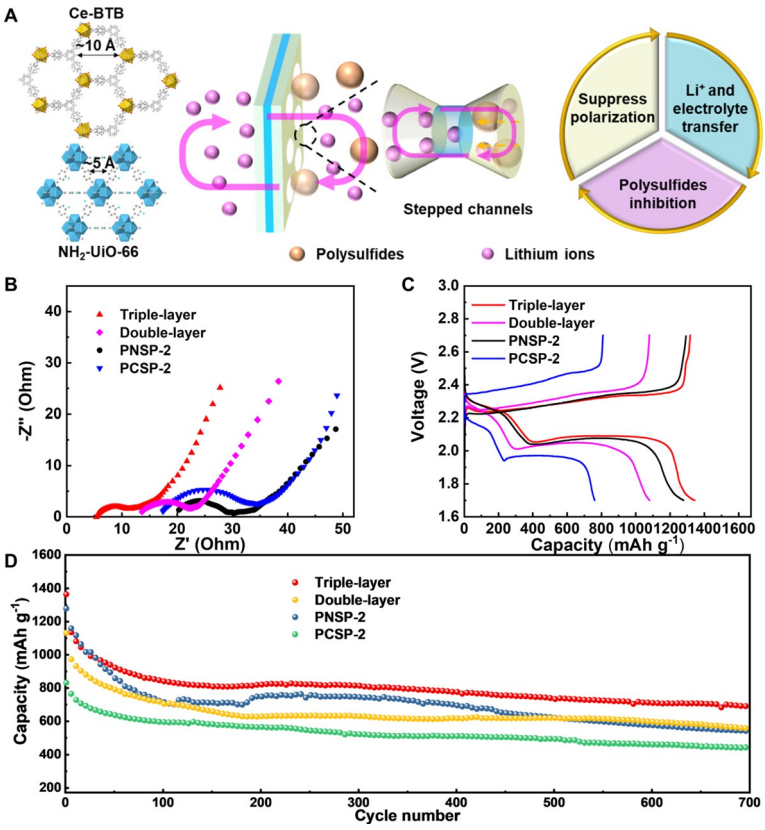

Figure 4. The performance of different separator-based Li-S cells. A) Representation of a triple-layer separator in the Li-S cell. B) Electrochemical impedance spectra of different separator-based Li-S cells. C) Galvanostatic charge–discharge profiles at the second cycle of different separator-based Li-S cells. D) Long-life cycling tests of different separator-based Li-S cells at 0.5 C.

The cycle stability is vital for the long-term application of Li-S battery. To further evaluate the long-term cycling stabilities, triple-layer membrane-based Li-S cell is carried out at 0.5 C. It has an initial capacity of 1365.0 mAh g^{-1} and the capacity in the 100th, 300th and 500th cycles are measured to be 843.9, 814.9, and 739.1 mAh g^{-1}, respectively (Figure 4D). The performance is better than both single-layer and double-layer membrane-based cells (double-layer, 618.8 mAh g^{-1}; PNSP-2, 621.1 mAh g^{-1}; PCSP-2, 494 mAh g^{-1}, at 500th, respectively) and is superior to most of reported MOF-based

separators (Table S2).[17] Besides, the capacity of triple-layer separator-based Li-S cell shows a stable curve from 100th to 700th cycle (0.03% fading per cycle; Figure 4D). As comparison, PP-based Li-S cell only exhibits an initial capacity of 979.4 mAh g^{-1} and rapidly decreases to 366 mAh g^{-1} with only 37% capacity retention after 700 cycles (Figure S27e). The triple-layer-based Li-S cell shows a high practical gravimetric energy density of 678 Wh kg^{-1} based on the total cell weight at 0.5 C. This result is moderate among reported practical gravimetric energy density as shown in Table S3.

To investigate the superiority of triple-layer-based separators over both single-layer and double-layer separators, chronoamperometry (CA) and lithium-ion diffusion coefficients tests have been conducted. The Li ion transference number (t_{Li+}) is evaluated via the combination of CA to study the Li^+ transfer ability.[41,42] The t_{Li+} of the separators are measured through the Li|separator|Li symmetric cell at room temperature. The triple-layer membrane-based separator exhibits a t_{Li+} of 0.55, which is higher than PNSP-2 (0.40) and double-layer separator (0.43), yet slightly lower than PCSP-2 (0.70). These results confirm the hypothesis that triple-layer separator with stepped channels would provide a large amount of available lithium-ion flux and raises the lithium ionic mass transfer rate between electrolyte (Figure 3C). In order to further study the polarization phenomenon caused by Li^+ transmission, galvanostatic cycling performances of symmetric Li|Li symmetric cells are charged/discharged at current density of 0.3 mA cm^{-2}. As shown in Figure 3D, compared with the other three membrane samples, the polarization voltage of the triple-layer separator-based Li|Li symmetric cell is only slightly larger than PCSP-2-based Li-S cell, indicating the low Li^+ transmission resistance. As mentioned above, triple-layer separator-based cell displays higher performance than PCSP-2-based Li-S cell, while the opposite results have been detected for the t_{Li+} values.[43] To distinguish the weird phenomenon, the lithium-ion diffusion coefficients of the Li-S battery are calculated based on the Randles–Sevcik equation (for the calculations see the Supporting Information; Figure S29). The lithium-ion diffusion coefficients indicate that the triple-layer with stepped channels separator-based Li-S battery provides the cell with stronger lithium-ion transfer capability ($D_{Li^+} = 5.63\times10^{-8}$ to 5.63×10^{-9} cm^{2}s^{-1}) when compared with that of PNSP-2 ($D_{Li^+} = 4.31\times10^{-8}$ to 3.52×10^{-9} cm^{2}s^{-1}), PCSP-2 ($D_{Li^+} = 1.85\times10^{-8}$ to 2.04×10^{-9} cm^{2}s^{-1}) and double-layer ($D_{Li^+} = 3.59\times10^{-8}$ to 3.10×10^{-9} cm^{2}s^{-1}). Above all, the specially designed triple-layer membrane-based separators can efficiently suppress the cell polarization, facilitate fast Li^+/electrolyte transfer and inhibit polysulfides shuttling, which possesses higher performance than both single-layer and double-layer-based separators. Besides, a batch of Li-S cells with higher sulfur loading (S content about 2.4 to 3 mg cm^{-2}) were assembled. Taking triple-layer separator with the optimized S content (2.4 mg cm^{-2}) as an example, the initial capacity is 1161.2 mAh g^{-1} at 0.05 C and decreases to 691.1 mAh g^{-1} after 29 cycles at 0.1 C, which proves the applicability of the triple-layer separator in Li-S battery with high S contents (Figure S30).

Conclusion

In conclusion, a two-step photoinduced heat-assisted processing (PHAP) method that can combine photoinduced shaping and heat-assisted solidification in a protocol has been proposed. The method enables shaping of MOFs into diverse devices (e.g., fiber, hollow tube, Janus hollow tube and double-layer/triple-layer membrane, etc.). For the first time, a kind of MOF-based triple-layer separator with stepped channels has been readily fabricated through the multidimensional fabrication of various MOFs. The powerful separator exhibits boosted specific capacity (1365.0 mAh g^{-1}) and cycling performance (0.03% fading per cycle from the 100th to 700th cycle) that is superior to pure PP, and single- and double-layer membranes. This is possibly due to the advantages of the MOF-based triple-layer membrane with stepped channels that can efficiently inhibit polysulfides shuttling, facilitate the fast transfer of Li^+/electrolyte and suppress cell polarization, as supported by sufficient characterization and comparative experiments. This work sheds fresh light on the exploration of functional MOF-based devices and brings new insight to the separator design for advanced Li-S batteries and analogous applications.

Acknowledgements

This work was financially supported by NSFC (No. 21871141, 21871142, 21701085 and 21901122), the NSF of Jiangsu Province of China (No. BK20171032), the Natural Science Research of Jiangsu Higher Education Institutions of China (No. 17KJB150025 and 19KJB150011), a project funded by the China Postdoctoral Science Foundation (No. 2018M630572 and 2019M651873), a Priority Academic Program Development of Jiangsu Higher Education Institutions, and the Foundation of Jiangsu Collaborative Innovation Center of Biomedical Functional Materials.

Conflict of interest

The authors declare no conflict of interest.

Keywords: Li-S battery · metal–organic frameworks · mixed matrix membranes · stepped channel separators

[1] R. Van Noorden, *Nature* **2014**, *507*, 26–28.
[2] G. Zhou, A. Yang, G. Gao, X. Yu, J. Xu, C. Liu, Y. Ye, A. Pei, Y. Wu, Y. Peng, Y. Li, Z. Liang, K. Liu, L.-W. Wang, Y. Cui, *Sci. Adv.* **2020**, *6*, eaay5098.
[3] Q. Pang, D. Kundu, M. Cuisinier, L. F. Nazar, *Nat. Commun.* **2014**, *5*, 4759.
[4] M. Shaibani, M. S. Mirshekarloo, R. Singh, C. D. Easton, M. C. D. Cooray, N. Eshraghi, T. Abendroth, S. Dörfler, H. Althues, S. Kaskel, A. F. Hollenkamp, M. R. Hill, M. Majumder, *Sci. Adv.* **2020**, *6*, eaay2757.
[5] Y. S. Su, A. Manthiram, *Nat. Commun.* **2012**, *3*, 1166.
[6] W. Xue, Z. Shi, L. Suo, C. Wang, Z. Wang, H. Wang, K. P. So, A. Maurano, D. Yu, Y. Chen, L. Qie, Z. Zhu, G. Xu, J. Kong, J. Li, *Nat. Energy* **2019**, *4*, 374–382.

[7] N. Li, Y. Xie, S. Peng, X. Xiong, K. Han, *J. Energy Chem.* **2020**, *42*, 116 – 125.
[8] D. Lin, Y. Liu, Y. Cui, *Nat. Nanotechnol.* **2017**, *12*, 194 – 206.
[9] J. Ryu, W. J. Song, S. Lee, S. Choi, S. Park, *Adv. Funct. Mater.* **2020**, *30*, 1902499.
[10] T. Li, X. Bai, U. Gulzar, Y. J. Bai, C. Capiglia, W. Deng, X. Zhou, Z. Liu, Z. Feng, R. Proietti Zaccaria, *Adv. Funct. Mater.* **2019**, *29*, 1901730.
[11] H. Qu, J. Zhang, A. Du, B. Chen, J. Chai, N. Xue, L. Wang, L. Qiao, C. Wang, X. Zang, J. Yang, X. Wang, G. Cui, *Adv. Sci.* **2018**, *5*, 1700503.
[12] M. Liu, N. Deng, J. Ju, L. Fan, L. Wang, Z. Li, H. Zhao, G. Yang, W. Kang, J. Yan, B. Cheng, *Adv. Funct. Mater.* **2019**, *29*, 1905467.
[13] W. G. Lim, S. Kim, C. Jo, J. Lee, *Angew. Chem. Int. Ed.* **2019**, *58*, 18746 – 18757; *Angew. Chem.* **2019**, *131*, 18920 – 18931.
[14] V. Lapornik, N. Novak Tusar, A. Ristic, R. K. Chellappan, D. Foix, R. Dedryvère, M. Gaberscek, R. Dominko, *J. Power Sources* **2015**, *274*, 1239 – 1248.
[15] F. Pei, L. Lin, A. Fu, S. Mo, D. Ou, X. Fang, N. Zheng, *Joule* **2018**, *2*, 323 – 336.
[16] L. Fan, M. Li, X. Li, W. Xiao, Z. Chen, J. Lu, *Joule* **2019**, *3*, 361 – 386.
[17] Y. He, Y. Qiao, Z. Chang, H. Zhou, *Energy Environ. Sci.* **2019**, *12*, 2327 – 2344.
[18] Z. Wang, W. Huang, J. Hua, Y. Wang, H. Yi, W. Zhao, Q. Zhao, H. Jia, B. Fei, F. Pan, *Small Methods* **2020**, *4*, 2000082.
[19] G. K. Gao, Y. R. Wang, H. J. Zhu, Y. Chen, R. X. Yang, C. Jiang, H. Ma, Y. Q. Lan, *Adv. Sci.* **2020**, *7*, 2002190.
[20] S. Bai, X. Liu, K. Zhu, S. Wu, H. Zhou, *Nat. Energy* **2016**, *1*, 16094.
[21] S. Bai, K. Zhu, S. Wu, Y. Wang, J. Yi, M. Ishida, H. Zhou, *J. Mater. Chem. A* **2016**, *4*, 16812 – 16817.
[22] A. Das, A. K. Thakur, K. Kumar, *Ionics* **2013**, *19*, 1811 – 1823.
[23] M. Tian, F. Pei, M. Yao, Z. Fu, L. Lin, G. Wu, G. Xu, H. Kitagawa, X. Fang, *Energy Storage Mater.* **2019**, *21*, 14 – 21.
[24] S. H. Kim, J. S. Yeon, R. Kim, K. M. Choi, H. S. Park, *J. Mater. Chem. A* **2018**, *6*, 24971 – 24978.
[25] C. Zhang, L. Shen, J. Shen, F. Liu, G. Chen, R. Tao, S. Ma, Y. Peng, Y. Lu, *Adv. Mater.* **2019**, *31*, 1808338.
[26] N. Deng, L. Wang, Y. Feng, M. Liu, Q. Li, G. Wang, L. Zhang, W. Kang, B. Cheng, Y. Liu, *Chem. Eng. J.* **2020**, *388*, 124241.
[27] C. Yan, X. B. Cheng, Y. Tian, X. Chen, X. Q. Zhang, W. J. Li, J. Q. Huang, Q. Zhang, *Adv. Mater.* **2018**, *30*, 1707629.
[28] R. Xu, Y. Xiao, R. Zhang, X. B. Cheng, C. Z. Zhao, X. Q. Zhang, C. Yan, Q. Zhang, J. Q. Huang, *Adv. Mater.* **2019**, *31*, 1808392.
[29] A. Knebel, P. Wulfert-Holzmann, S. Friebe, J. Pavel, I. Strauss, A. Mundstock, F. Steinbach, J. Caro, *Chem. Eur. J.* **2018**, *24*, 5728 – 5733.
[30] M. S. Denny, Jr., M. Kalaj, K. C. Bentz, S. M. Cohen, *Chem. Sci.* **2018**, *9*, 8842 – 8849.
[31] Y. Chen, X. Huang, S. Zhang, S. Li, S. Cao, X. Pei, J. Zhou, X. Feng, B. Wang, *J. Am. Chem. Soc.* **2016**, *138*, 10810 – 10813.
[32] J. Kang, J. B. H. Tok, Z. Bao, *Nat. Electron.* **2019**, *2*, 144 – 150.
[33] L. Duan, W. Kong, W. Yan, C.-H. Li, Z. Jin, J.-L. Zuo, *Sustainable Energy Fuels* **2020**, *4*, 2760 – 2767.
[34] K. S. Park, Z. Ni, A. P. Côté, J. Y. Choi, R. Huang, F. J. Uribe-Romo, H. K. Chae, M. O'Keeffe, O. M. Yaghi, *Proc. Natl. Acad. Sci. USA* **2006**, *103*, 10186 – 10191.
[35] S. R. Venna, M. A. Carreon, *J. Am. Chem. Soc.* **2010**, *132*, 76 – 78.
[36] J. Cravillon, S. Münzer, S.-J. Lohmeier, A. Feldhoff, K. Huber, M. Wiebcke, *Chem. Mater.* **2009**, *21*, 1410 – 1412.
[37] W. Liang, F. Lian, N. Meng, J. Lu, L. Ma, C.-Z. Zhao, Q. Zhang, *Energy Storage Mater.* **2020**, *28*, 350 – 356.
[38] Q. Fan, W. Liu, Z. Weng, Y. Sun, H. Wang, *J. Am. Chem. Soc.* **2015**, *137*, 12946 – 12953.
[39] S. Xin, L. Gu, N. H. Zhao, Y. X. Yin, L. J. Zhou, Y. G. Guo, L. J. Wan, *J. Am. Chem. Soc.* **2012**, *134*, 18510 – 18513.
[40] G. Zhou, S. Pei, L. Li, D. W. Wang, S. Wang, K. Huang, L. C. Yin, F. Li, H. M. Cheng, *Adv. Mater.* **2014**, *26*, 625 – 631, 664.
[41] Y. Li, W. Wang, X. Liu, E. Mao, M. Wang, G. Li, L. Fu, Z. Li, A. Y. S. Eng, Z. W. Seh, Y. Sun, *Energy Storage Mater.* **2019**, *23*, 261 – 268.
[42] Z. A. Ghazi, X. He, A. M. Khattak, N. A. Khan, B. Liang, A. Iqbal, J. Wang, H. Sin, L. Li, Z. Tang, *Adv. Mater.* **2017**, *29*, 1606817.
[43] S. H. Chung, A. Manthiram, *Adv. Energy Mater.* **2019**, *9*, 1901397.

Manuscript received: December 14, 2020
Revised manuscript received: January 13, 2021
Accepted manuscript online: January 28, 2021
Version of record online: March 18, 2021

